Atmósfera (1991), **4**, *pp. 101-115*

Wind-induced circulation in Todos Santos bay, B. C., Mexico

M. L. ARGOTE ESPINOZA, F. J. GAVIDIA MEDINA and A. AMADOR BUENROSTRO

Departamento de Oceanografía Física, CICESE, Apartado Postal 2732, Ensenada, B. Cfa., Mézico

(Manuscript received June 29, 1990; accepted in final form October 1, 1990)

RESUMEN

Un modelo numérico hidrodinámico es usado para predecir la circulación del viento inducido en la Bahía de Todos Santos por las condiciones representativas del viento de verano, invierno y los vientos irregulares "Santana", del Oeste. Las máximas velocidades a lo largo de la costa y corrientes de retorno, son aparentemente inducidas por efectos topográficos. Algunos efectos de esta circulación son discutidos en relación a los problemas de contaminación.

ABSTRACT

A hydrodynamical numerical model is used to predict the wind-induced circulation in Todos Santos Bay for wind conditions representative of summer, winter and the aperiodic westerly "Santana" winds. Maximum velocities along the coast and return flows are apparently induced by topographic effects. Some effects of this circulation are discussed in relation to pollution problems.

Introduction

Todos Santos Bay (Fig. 1) is located on the northwest coast of the Baja California Peninsula, with a surface of ~200 km^2. Its communication with the open sea (~20 km wide) is limited by the Todos Santos Islands, located about 7 km off Punta Banda. The bathymetry consists of a shallow (mean depth ~30 m), relatively smooth bottom, except for the ~400 m deep abrupt canyon located between Punta Banda and the Todos Santos Islands.

Although there are a number of studies of the Bay, dealing with aspects of biology, pollution and chemistry among other, those related to the hydrodynamics are scarce and have been exclusively observational. The only current measurements reported for this region are sea surface lagrangean measurements near the coast (Alvarez *et al.*, 1988) and a current-meter data report of a meter located near Estero de Punta Banda sand bar (Ocampo, 1983). Previously, attempts were made to obtain circulation patterns based on temperature and salinity distributions (Argote *et al.*, 1975). Seasonal variations of the sea surface current reported by Alvarez *et al.* (1988), ~0.15 m s^{-1} for the period March-August and ~0.05 m s^{-1} for the period September-January, are apparently associated with seasonal variations of wind stress. Tidal streams in the Bay, with maximum velocities of about 0.015 m s^{-1} for the most energetic harmonic M2, and tidally induced residual currents of the order of 10^{-4} m s^{-1} (Gavidia, 1988) have a negligible effect on the circulation.

It is apparent from these studies that the wind is the prime driving force of the circulation in the Bay. In this paper, a hydrodynamical numerical model is used to predict the wind-induced circulation, and the confidence in the predictions is tested by comparison against direct measurements.

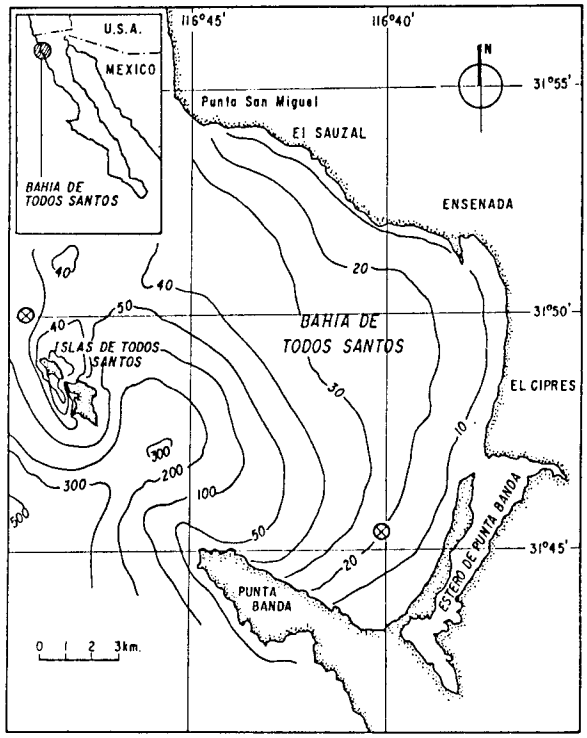

Fig. 1. Bathymetry of Todos Santos Bay, Baja California. Depth contours are in meters.

Table I. Symbols used in the text

C_b = drag coefficient for bottom stress
C_w = drag coefficient for wind stress
Dt = time step
Dx, Dy = lenght step in the x and y direction, respectively
f = Coriolis parameter
$F_w = \tau_w / \rho_w$
g = acceleration due to the gravity
H = depth of bottom below level reference surface
H_{max} = maximum depth inside the area modelled
$H + \eta$ = total water depth
K_h = hrizontal kinematic eddy viscosity
t = time coordinate
u, v = vertically integrated horizontal water velocities in x and y directions respectively
U, V = vertically integrated transport in the x and y directions respectively
W = wind velocity
x, y = horizontal coordinates (right hand axes)
∇_h^2 = the two dimensional Laplacian operator
η = sea surface elevation
τ_b = bottom stress
τ_w = wind stress
τ_{wx}, τ_{wy} = wind stress along the x and y direction respectively
ρ_a = air density
ρ_w = sea water density

The model

The two-dimensional hydrodynamical numerical model developed by Hunter (1980) was used to

predict the currents induced by a steady wind stress. This model solves the vertically integrated-equations of momentum and continuity (the symbols used are defined in Table I):

$$\frac{\partial u}{\partial t} = -u\frac{\partial u}{\partial x} - v\frac{\partial u}{\partial y} - g\frac{\partial \eta}{\partial x} + fv + \frac{\tau_{wx} - \tau_{bx}}{\rho_w(H+\eta)} + K_h(\nabla_h^2 u) \tag{1}$$

$$\frac{\partial v}{\partial t} = -u\frac{\partial v}{\partial x} - v\frac{\partial v}{\partial y} - g\frac{\partial \eta}{\partial y} - fu + \frac{\tau_{wy} - \tau_{by}}{\rho_w(H+\eta)} + K_h(\nabla_h^2 v) \tag{2}$$

$$\frac{\partial \eta}{\partial t} = -\frac{\partial (H+\eta)u}{\partial x} - \frac{\partial (H+\eta)v}{\partial y} \tag{3}$$

In the above equations bottom stress (τ_b) and wind stress (τ_w), are parameterized by the following relations:

$$\underline{\tau_b} = \rho_w C_b \underline{v} \mid \underline{v} \mid \qquad \underline{\tau_w} = \rho_a C_w \underline{W} \mid \underline{W} \mid \tag{4}$$

where $\underline{v}$ is the vertically averaged velocity and $\underline{W}$ is the wind velocity vector.

The equations are solved by conventional finite differences using an explicit scheme, therefore the main stability requirement to be met is the CFL criterion (Courant, Friedrich and Lewy, 1928) which for this case is:

$$Dt < \frac{1}{\sqrt{gH_{\max}(Dx^{-2} + Dy^{-2}}} \tag{5}$$

where $H_{\max}$ is the maximum depth inside the area modelled, Dx and Dy are the grid size in the x and y directions, respectively, and Dt is the time step. In the diffusion term, the horizontal eddy viscosity K_h was set arbitrarily at 10 m^2 s^{-1}.

Input data

A 1.0 km × 1.0 km grid was chosen, with the y axis oriented in a direction of 304°N, along the main axis of the Bay (Fig. 2). The bathymetry was digitized from the Chart 120-16-4, zone R-11 (1971). As the maximum depth of the modelled area was 585 m, a time step of 8.94 seconds was chosen to satisfy the CFL stability requirement.

Winds in the Baja California NW coast present seasonal variations associated to changes in position and strength of a low pressure centre located off the west coast. The gradient between those two pressure centres increases during spring and summer, giving as a result strong north winds. Weaker winds in winter with variable direction result from reduced pressure gradients between these two pressure centres (Reid *et al.*, 1958).

Studies of local winds in the Bay (Reyes *et al.*, 1983) suggest a lack of correlation between winds obtained from surface pressure maps and those measured along the coast. This is due mainly to local thermal instabilities, frictional effects and differences in energy dissipation. Local thermal instabilities induce strong sea-land breezes which represents the highest energy in wind

records. Frictional effects over the ground and differences of energy dissipation in the sea-land boundary (higher over land than over the sea) reduce the wind speed. Less marked differences were obtained by these authors when the comparisons were made with wind measurements at Todos Santos Islands.

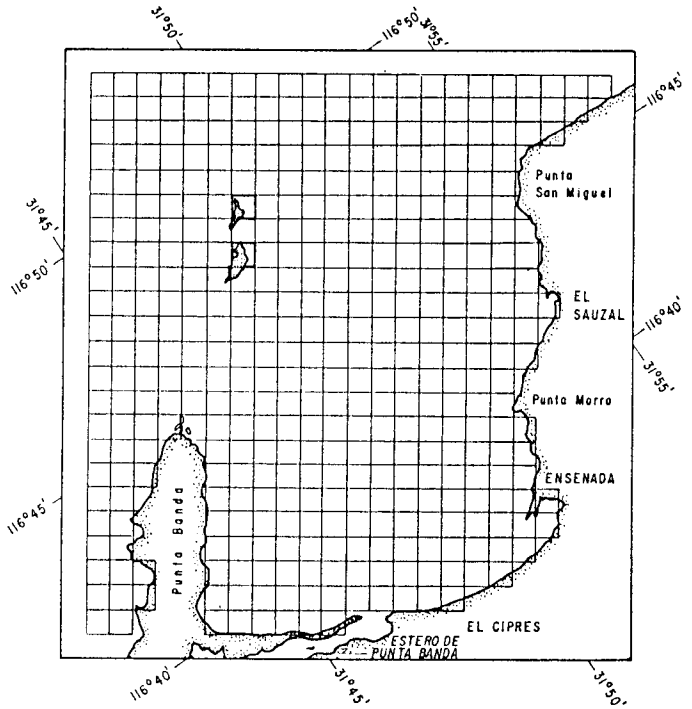

Fig. 2. The 1 km × 1 km grid used in the numerical model.

Table II. Wind stress used as input in the model, wind stress was assumed to be related to the wind W_{10} at a height of 10 m, by the relation $\tau_w = \rho_w C_{10} W_{10} \mid W_{10} \mid$. Drag coefficient values C_{10} were obtained from Phillips (1977).

	Wind speed m s^{-1}	Wind directions	Drag Coefficient C_{10}	Wind stress N m^{-2}
SUMMER	5	NW, W, N	0.011	0.034
WINTER	1	S, SW	0.013	0.0016
SANTANA	10	E	0.013	0.160

Table II indicates the wind speeds and directions used to estimate the wind stress used in the model. To take into account frictional effects, the wind speeds are about 30% lower than those reported by Reyes *et al.* (1983) for Todos Santos Islands. The model results were derived in terms of wind stress rather than wind speed.

A steady wind stress was imposed on a working model of the M2 tide. The tidal flow was driven by prescribing, along the open sea boundary homogeneous values of elevation (0.487 m) and phase (265°) of the M2 (obtained from Godin *et al.*, 1980). A fixed bottom friction coefficient $C_b = 0.003$ was used.

The model was started with all speeds and elevations inside the interior grid points set to zero. At the coastline, the normal velocity was set to zero and free-slip conditions were imposed for the tangential velocity. Maximum differences of about 2.5% in the amplitude of u and v and η between the 4th and 5th cycle suggest convergence of the numerical solution. Residual flows and sea levels due to wind forcing were determined by averaging over a tidal cycle, once the solution had converged and the residual pattern had achieved a steady state.

Results

For the wind conditions considered (Figs. 3 to 5) maximum current velocities are predicted along the coast in a band ~3 km wide, contrasting with the relatively weak offshore flow directed to the right of the wind.

For summer NW, W and N winds (Fig. 3) the model predicts flow into the Bay along the Punta San Miguel coast. This coastal flow has been also suggested by lagrangean measurements (Alvarez *et al.*, 1988) and inferred from temperature and salinity distributions (Argote *et al.*, 1975) under similar wind conditions.

For NW and N winds (Figs. 3a and 3c), flow into the Bay is along both Punta Banda and Punta San Miguel coasts, and areas of convergence are clearly evident. The position of these convergence zones appears to be dependent on the wind direction. A change of 45° on the wind direction from NW to N precludes the formation of the convergence.

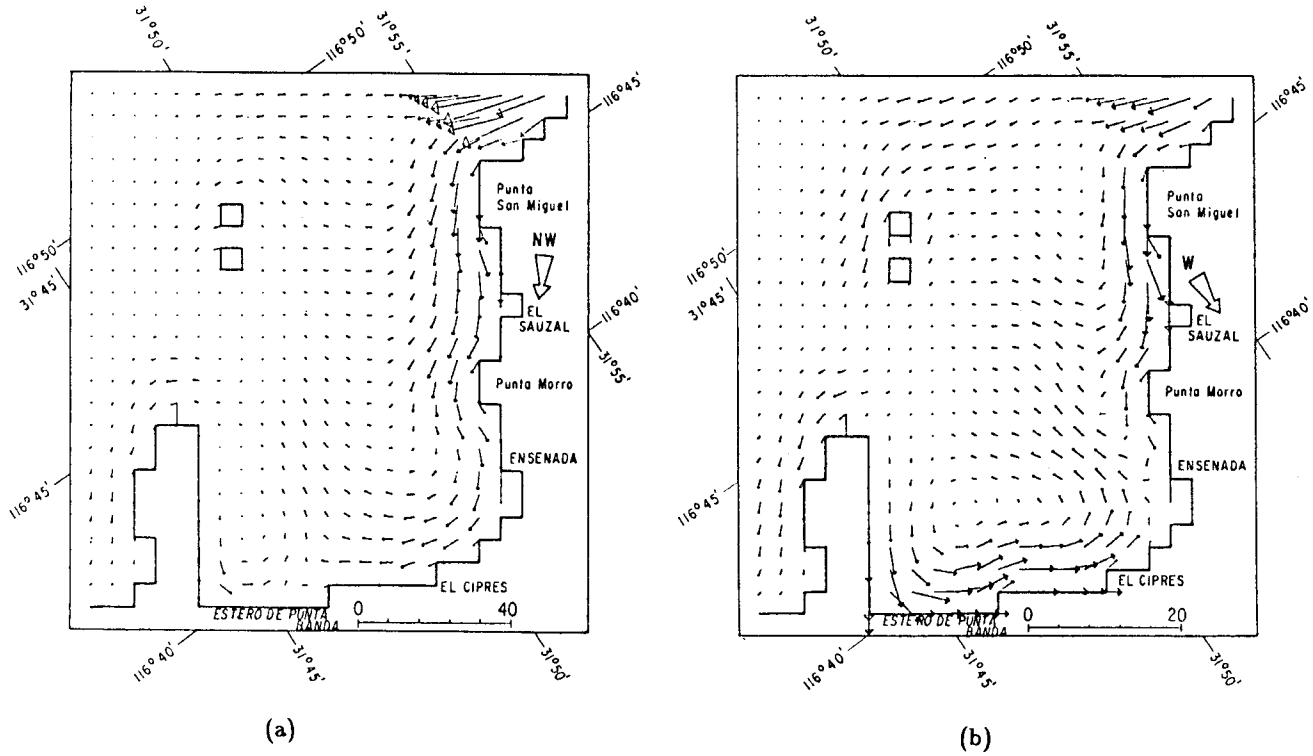

Fig. 3. Wind-driven residual currents predicted for a uniform 0.034 N m^{-2} wind-stress for the directions (a) NW, (b) W and (c) N, representative of summer wind conditions. Units are cm s^{-1}.

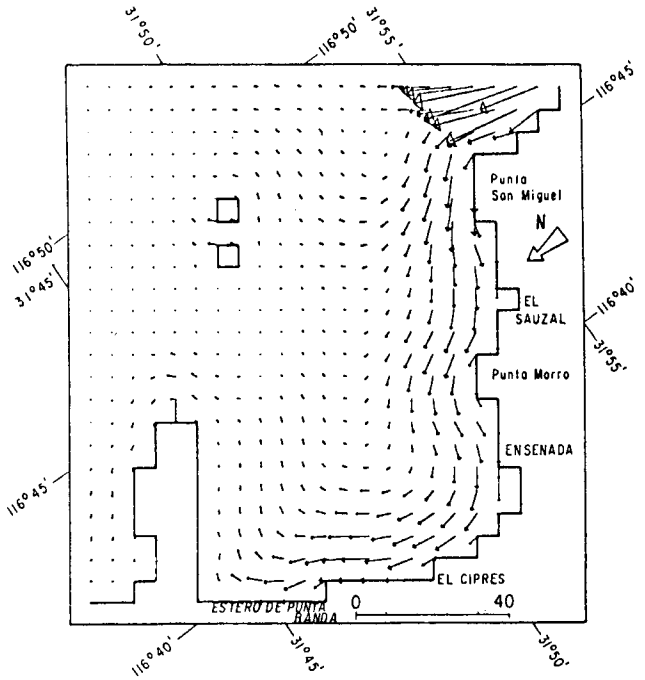

(c)

Figure 3 (continued)

Analysis of relative vorticity and divergence based on drogue measurements (Durazo and Alvarez, 1988), suggest convergence in the area adjacent to the sand bar of Estero de Punta Banda, where convergence is also predicted by this model NW winds (Fig. 3a).

For winter S and SE and Santana (E) winds (Figs. 4 and 5), flow along Punta San Miguel

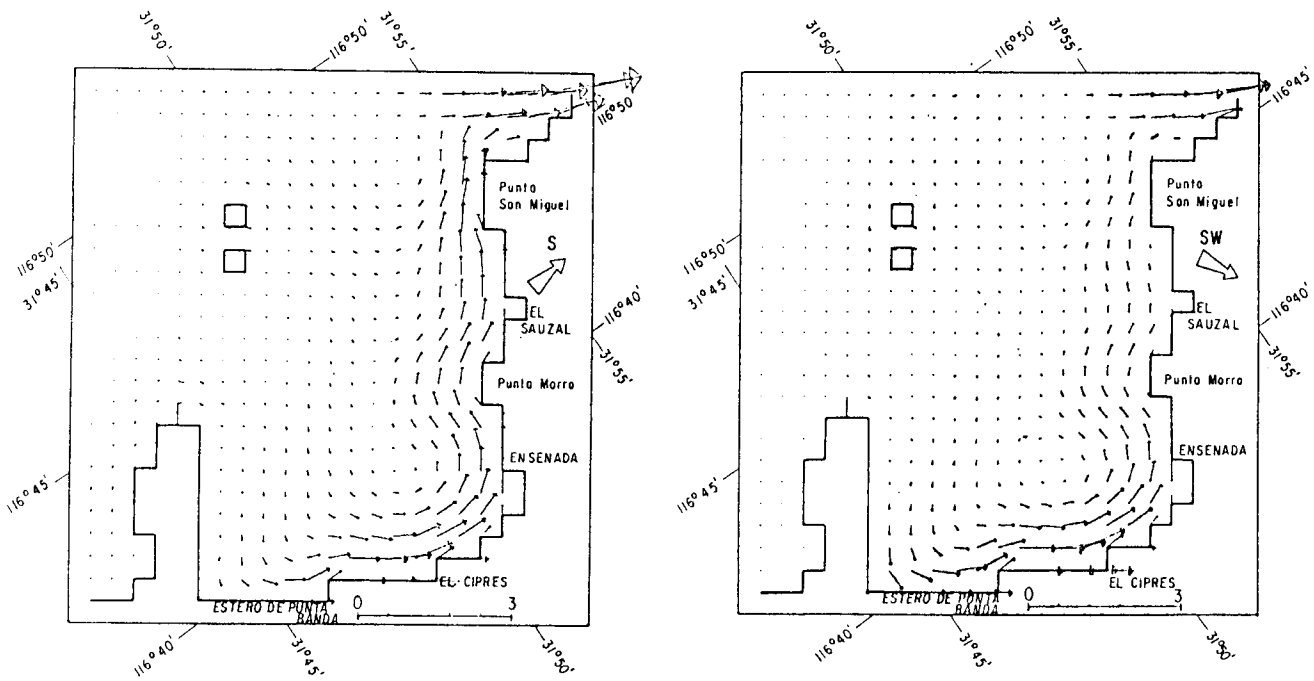

Fig. 4. Wind-driven residual currents predicted for a uniform 0.0016 N m^{-2} wind-stress for the directions (a) S and (b) SW, representative of winter conditions. Units are cm s^{-1}.

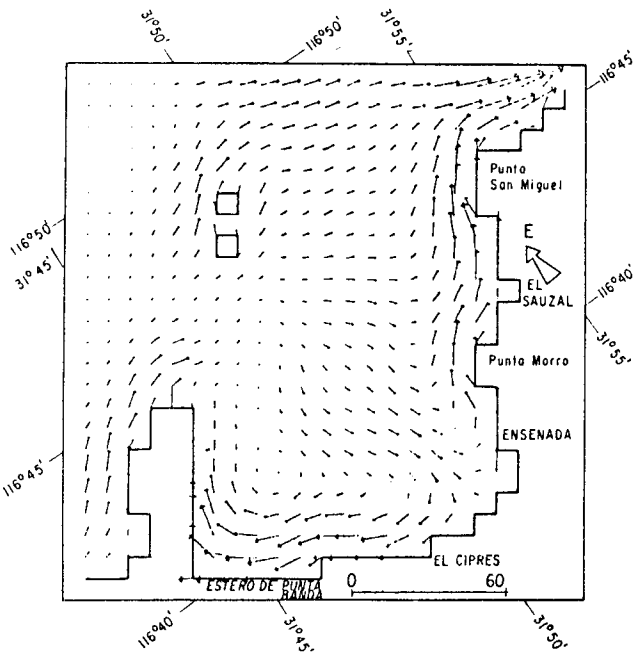

Fig. 5. Wind-driven residual currents predicted for a uniform E wind-stress of 0.16 N m^{-2}, representative of the aperiodical "Santana Condition". Units are cm s^{-1}.

coast is in opposite direction to that predicted for the summer winds as a result of opposite wind directions. The general circulation pattern resulting from wind blowing exactly in opposite directions (W and E; Figs. 3b and 5) induce the same circulation patterns but with directions reversed. Maximum velocities predicted for E winds are the result of applying maximum wind stress.

Discussion

The relative importance of each term included in the numerical model, neglecting momentum advection and diffusion, can be assessed through estimates of the order of magnitude of each term:

Advection terms:

$$v\frac{\partial v}{\partial y} \sim 0[(5.5 \times 10^{-2})\left(\frac{2.0 \times 10^{-2}}{1000}\right)] \sim 0[1.0x10^{-6}]\text{ms}^{-2}$$

where $\frac{\partial v}{\partial y} = 2.0 \times 10^{-2}$ s^{-1} is the maximum velocity gradient on the boundary of the high speed coastal zone, and $v = 5.5 \times 10^{-2}\text{ms}^{-2}$ is the maximum velocity near the coast.

Coriolis force:

$$fkv \sim 0[(7.69 \times 10^{-5})(5.5 \times 10^{-2})] \sim 0[4.2 \times 10^{-6}]\text{ms}^{-2}$$

where $v = 5.5 \times 10^{-2}$ ms^{-1}, is the maximum velocity near the coast.

Pressure gradient:

$$g\nabla\eta \sim 0[9.81(1.8 \times 10^{-7})] \sim 0[1.8 \times 10^{-6}]\text{ms}^{-2}$$

where $\nabla\eta = 1.8 \times 10^{-7}$, is the sea surface gradient near the coast.

Wind stress:

$$\frac{C_s \rho_a W \mid W \mid}{\rho_w H} \sim 0\left[\frac{(1.1 \times 10^{-3})(1.25)(5)^2}{(1026.0)(20)}\right] \sim 0[1.7 \times 10^{-6}]\text{ms}^{-2}$$

For wind speed of 5 m s^{-1}.

Bottom friction:

$$\frac{C_b V \mid V \mid}{H} \sim 0\left[\frac{3.0 \times 10^{-3}(5.5 \times 10^{-2})^2}{20}\right] \sim 0[4.6 \times 10^{-7}]\text{ms}^{-2}$$

For water depth of 20 m and maximum velocity 5.5×10^{-2} m s^{-1}.

Diffusion term:

$$K_h(\nabla_h^2 v) \sim 0[10 \times 2.5 \times 10^{-8}] \sim 0[2.5 \times 10^{-7}]\text{ms}^{-2}$$

where $\nabla_h^2 v = 2.5 \times 10^{-8}$ m^{-1} s^{-1} was estimated at the boundary of the high speed coastal band.

It is evident that diffusion and bottom friction terms (one order of magnitude smaller than the remaining terms) have a restricted effect in the momentum balance. Bottom friction will play an important role only over water depths less than 10 m, whereas diffusion term effect will be restricted to the edge of the high speed coastal band. The diffusion term can also be neglected, based on the consideration that it was included in the model mainly for the sake of numerical stability, and although it describes a physical process it is, generally smaller than the other terms in the momentum equation.

The advection term, although of the same order of magnitude than Coriolis force, pressure gradient and wind stress, can be neglected in the momentum equation to provide sufficient simplicity necessary for the foregoing discussion. The reason for this linearization is partly that the momentum advection terms have the form of a divergence and that vanishes on approaching the boundaries. Thus, their role is to transfer momentum from one region of the basin to another, without modifying the total moment input (Csanady, 1984).

Comparison between the numerical model results with analytical models

The behaviour of the wind-induced circulation patterns predicted by the numerical model can also be analysed by comparison against analytical models, which allow physical insight into the mechanisms generated by the wind stress over a shallow basin.

The balance between wind stress, Coriolis force and pressure gradient can be analyzed by means of a simplified model by Csanady (1984) in terms of the horizontal transports, defined as:

$$U = \int_{-H}^{o} u dz; \qquad V = \int_{-H}^{o} v dz \tag{6}$$

Here, the small surface elevation changes $\eta(x, y)$ are neglected in comparison with the mean depth $H(x, y)$.

a) Constant depth basin

The most simplified case is that of a constant depth closed basin, over which a uniform wind stress F_{wx} acts along the x direction ($F_{wy} = 0$). The coast in this basin will prevent normal transport and, as a first approximation, sea level changes at points near the coast may be determined, based on the hypothesis that both transport components vanish everywhere $U = V = 0$. The momentum equations under these assumptions can be reduced to:

$$0 = -gH\frac{\partial \eta}{\partial x} + F_{wx}, \tag{7}$$

$$0 = -gH\frac{\partial \eta}{\partial y}, \tag{8}$$

$$0 = -\frac{\partial \eta}{\partial t}, \tag{9}$$

and the solution is:

$$\eta = \frac{F_{wx}x}{gH} \tag{10}$$

This solution represents a simple balance of forces between wind stress and horizontal gradient of pressure associated with the sea level slope which in this case is inversely proportional to the

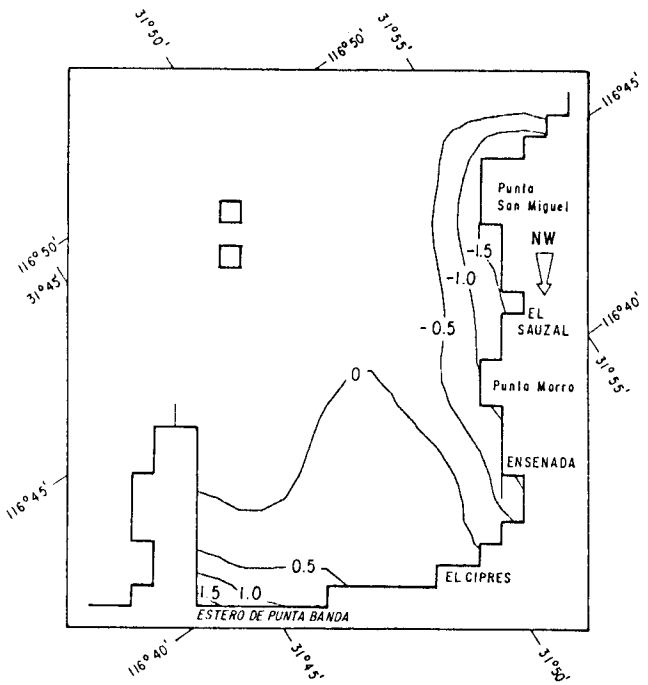

Fig. 6. Sea level corresponding to the NW wind residuals shown in Fig. 3a. Units are mm.

depth of the basin. Wind stress in this analytical model can be related to the numerical model by $F_w = \tau_w/\rho_w$.

As an example, we can analyse the inner corner of the Bay, formed by the sand bar and Punta Banda where for NW wind (Figs. 3a and 6), the residuals are small and maximum sea surface slope $\approx 1.8 \times 10^{-7}$ m is predicted. The water depth in this region is ≈ 20 m, which gives, from equation 10, $\Delta\eta \sim 1.7 \times 10^{-7}$ m. Therefore in this zone the sea surface slope just balances the wind stress, and the vertically integrated residual flow resulting from this balance falls to zero.

b) Variable depth basin

A more realistic approach to real conditions is achieved by including variable bottom topography, as is the case of a long narrow closed basin with parallel depth contours over a substantial extension of the basin. The x axis is oriented along its length (Fig. 7), along which a constant wind stress F_{wx} is suddenly imposed at time $t = 0$. Along the parallel contours of the basin,

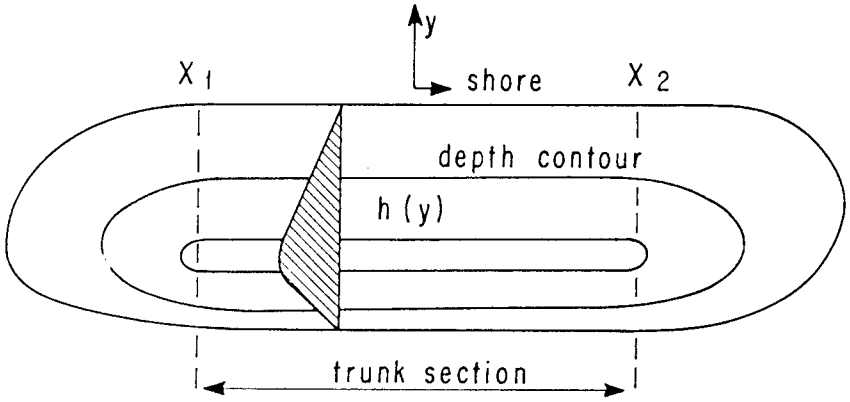

Fig. 7. Schematic diagram of a shallow sea with regular 'trunk' section, in which depth contours are parallel. From Csanady (1984).

as $F_{wy} = 0$ it is assumed that $V = 0$. If Earth rotation effects are considered unimportant, the linearized transport equation in the region $x_1 < x < x_2$), with Coriolis force and bottom stress neglected can be reduced to:

$$\frac{\partial U}{\partial t} = -gH\frac{\partial \eta}{\partial x} + F_{wx} \qquad x_1 < x < x_2 \tag{11}$$

$$0 = gH\frac{\partial \eta}{\partial y} \qquad x_1 < x < x_2 \tag{12}$$

$$\frac{\partial U}{\partial x} = -\frac{\partial \eta}{\partial t} \qquad x_1 < x < x_2 \tag{13}$$

where $H = H(x, y)$.

From these equations Csanady (1984) (after a series of considerations and integrating over the

across section of the basin, y_1 to y_2) obtained the following expressions for the gradient elevation and the transport in the cross section:

$$\frac{\partial \eta}{\partial x} = \frac{F_{wx} b}{gS} \qquad x_1 < x < x_2 \tag{14}$$

$$U = F_{wx} t \left[1 - \frac{Hb}{S}\right] \tag{15}$$

where

$$b = y_2 - y_1$$

is the width of the basin and

$$S = \int_{y_2}^{y_1} H dy$$

is the cross sectional area.

Equation 15 shows that the downwind transport (U) is proportional to $F_{wx}t$, which is the impulse of the wind stress. The transport is zero where $H = S/b$ which is the average depth of the section. Along this average depth, wind stress and pressure gradient are in exact balance and no flow is induced, as in the above case of constant depth. In shallow waters where $Hb < S$, wind stress is greater than the gravity force $gH\partial\eta/\partial x$ due to surface slope, and the water accelerates downwind. In deep waters ($Hb/S > 1$) the pressure gradient dominates and return flows develop.

Under these conditions, the circulation develops with flow in the wind direction nearshore and reduced return flow in deeper waters. The relatively strong coastal flow predicted by the numerical model (Figs. 3 to 5) can be explained in terms of the above results.

Table III. Mean velocity obtained from the numerical model for sections 3 km wide, off Punta San Miguel (PSM), Punta Banda (PB) and Todos Santos Islands (TSI). H is the section mean depth. Underlined values marked with (*), indicate wind stress acting for a 10 hour period, over H (eq. 15).

		Velocity in cm s^{-1}		
Wind stress N m^{-2}	Wind direction	PSM H = 45 m	PB H = 135 m	TS H = 78 m
0.034	NW	5.1	1.7	1.0
	W	1.9	1.0	1.4
	N	5.5	0.9	1.4
		2.6*	0.9*	1.5*
0.0016	SW	0.1	0.1	0.1
	S	0.3	0.1	0.1
		0.12*	0.04*	0.07*
0.16	E	7.6	5.7	5.6
		12.5*	4.2*	7.3*

Comparisons between currents predicted by the numerical model and those calculated by equation 15 are presented in Table III. The numerical model values represent the average current over a 3 km wide section for regions near Punta San Miguel (PSM), Punta Banda (PB) and Todos Santos Islands (TSI). Values obtained from equation 15 correspond to wind stress ($F_{wx}t$) acting during a 10 hours period distributed over the mean depth (H) of the section.

These comparisons show satisfactory agreement, taking into consideration the simplifications of the analytical model. This supports the proposed importance of topographic effects, which appear to be responsible of the presence of relatively strong currents and return flows in the coastal band.

c) Coriolis force effect

Outside the coastal band the relatively weak flow directed to the right of the wind suggests that Coriolis force could be important on this area. Over this offshore region once the steady state is reached, the sea surface is flat (Fig. 6). This condition can be analyzed assuming that motion is forced by a wind stress F_{wy} applied along the y axis of a basin. The linearized transport equations for steady state conditions, neglecting bottom stress are reduced to:

$$-fV = 0 \tag{16}$$

$$fU = F_{wy} \tag{17}$$

$$\frac{\partial u}{\partial x} + \frac{\partial V}{\partial y} = 0 \tag{18}$$

These equations are satisfied by:

$$U = \frac{F_{wy}}{f} = \text{constant} \tag{19}$$

$$V = 0 \tag{20}$$

Equation 19 indicates that vertically integrated transport, with magnitude F_{wy}/f, is directed at right angles to the wind direction (in the Northern Hemisphere) as the result of the balance between the wind stress and the Coriolis force. According to the current patterns predicted by the numerical model, this balance appears to dominate the dynamics of the area off the coastal band (Figs. 3 to 5).

Implications of the circulation in relation to pollution of the Bay

If, as it has been indicated (Sañudo and Vargas, 1984), maximum industrial discharges in Todos Santos Bay, occur during summer months in the northern part of the Bay, it is evident from the summer circulation patterns (Fig. 3) that these discharges will be transported towards the interior of the Bay, while in winter and during Santana winds, the transport would be towards the open

sea (Figs. 4 and 5). A rough estimate of the time spent by a particle inside the Bay, released in the vicinity of Punta San Miguel during the summer months, is about 7 days, since the particle would be carried by the current over a distance ~20 km at a velocity of ~3 cm s^{-1}, assuming a steady state.

The relative concentration of contaminants in the Bay can be assessed by means of estimates of the pollution susceptibility parameter (PS). This parameter is defined as the reciprocal of the volume of water that passes during one day through a line extending from the shore to a distance of one kilometer, regardless of the direction of the flow (Weyl, 1976). High values (1000 km^3 day^{-1}) are expected in areas of reduced transport and/or shallow depth, while in those of strong transport and/or deep water low values (1 km^3 day^{-1}) will be expected.

Distribution of PS for summer wind conditions are shown in Figure 8. Maximum values (900 km^3 day^{-1}) are estimated for coastal areas adjacent to the north of Punta San Miguel, El Sauzal, the Harbor and Punta Banda, while values lower than 10 km^3 day^{-1}, are found in areas of strong velocity on the south coast, off San Miguel and in deep regions (the canyon zone and outside the Bay).

These results suggest that for summer wind conditions, along the coastal zone south of Punta San Miguel, strong transport would prevent accumulation of industrial or domestic discharges, since these would be transported along the coast to the interior of the Bay; while in those areas to the north of punta San Miguel, El Sauzal and the Harbor, substances introduced to the Bay by industrial and domestic discharges would remain and could be concentrated due to the reduced transport.

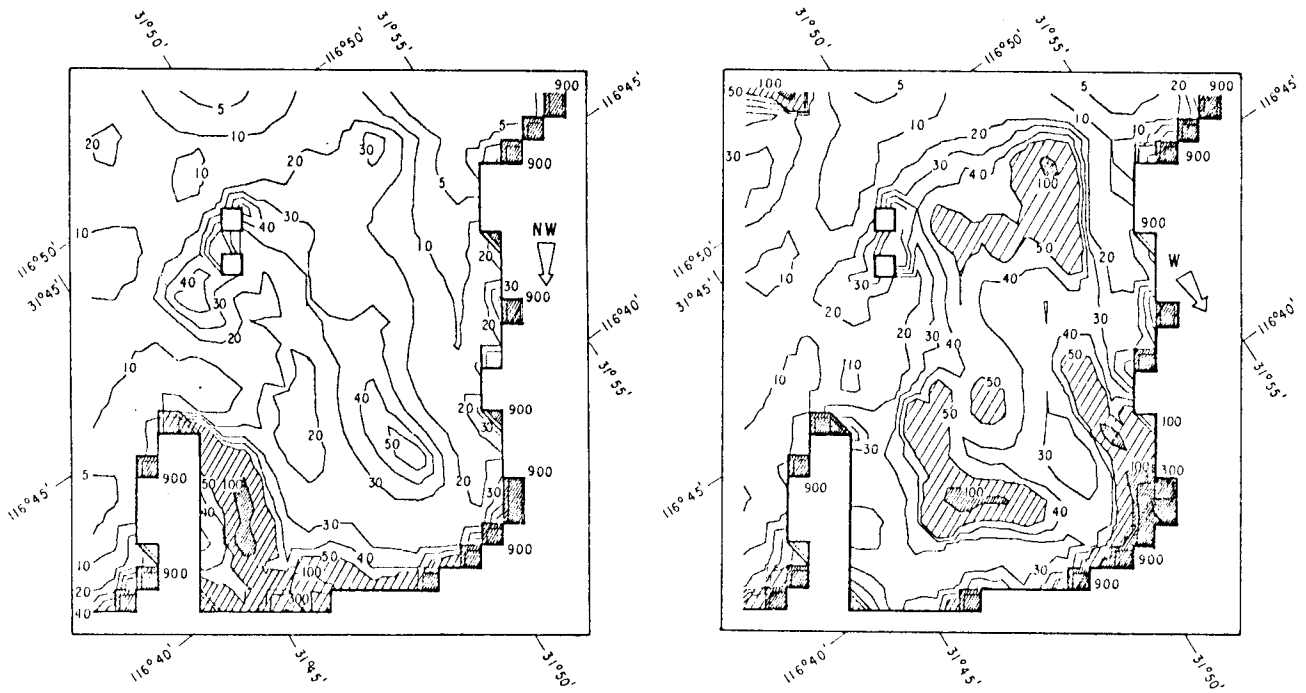

Fig. 8. Pollution susceptibility parameter (PS) calculated from the wind-driven residual currents shown in Fig. 3 for: (a) NW, (b) W and (c) N winds. Units are km^3 day^{-1}.

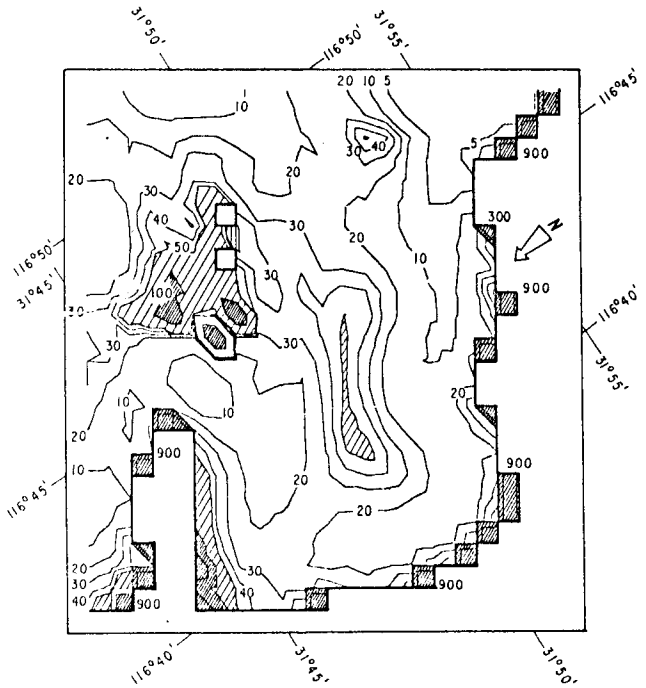

(c)

Figure 8 (continued)

Conclusions

The model reproduces satisfactorily the main features of the circulation indicated by the available direct measurements, such as coastal flow and convergence areas, which are apparently induced by topographic effects. The presence and the geographic position of return flows are highly sensitive to the wind direciton. The flow off Punta San Miguel reverses its direction, with inflow during the summer and outflow during the winter. This circulation pattern will strongly influence the geographic and seasonal distribution of industrial and domestic discharges. Direct measurements to improve the confiability of the numerical predictions are highly desirable. These will hopefully be provided by current meter measurements in progress.

Acknowledgements

We would like to thank Dr. John R. Hunter for permitting the use of his numerical model. Thanks are due to Dr. Miguel F. Lavin, Dr. Pedro Ripa, and M. Sc. Luis G. Alvarez for helpful comments on the manuscript and to J. Favián Cabrera S. and José Ma. Domínguez O. for their help with the figures. This study was supported by the Secretaría de Programación y Presupuesto (SPP), through CICESE founding; student grants were provided by CONACYT and CICESE.

REFERENCES

Alvarez Sánchez, L. G., R. Hernández y R. Durazo, 1988. Patrones de deriva de trazadores lagrangeanos en la Bahía de Todos Santos. *Ciencias Marinas,* **14**(4), 135-162.

Argote Espinoza, M. L., A. Amador y C. Morales, 1975. Distribución de los parámetros salinidad y temperatura y tendencias de la circulación en Bahía de Todos Santos, B. C., Memorias de la primera reunión del CIBCASIO: 3-30.

Csanady, G. T., 1984. Circulation in Coastal Ocean. D. Reidel Company, 279 pp.

Courant, R., K. Friedrichs and H. Lewy, 1928. Über die partiellen differenzengleichungen der mathematischen physik, *Math. Ann.* **100**, 32-74.

Durazo Arvizu, R. y L. G. Alvarez Sánchez, 1988. Cinemática de la región sur de la Bahía de Todos Santos, B. C., *Ciencias Marinas*, **14**(1), 95-144.

Gavidia Medina, F. J., 1988. Simulación numérica de la circulación barotrópica en la Bahía de Todos Santos, B. C., M. Sc. thesis, Centro de Investigación Científica y Educación Superior de Ensenada Baja California, 95 pp.

Godin, G., R. De La Paz-Vela, N. Rodríguez y M. Ortiz, 1980, Revisión de los datos de mareas de la costa Occidental de México disponibles en el CICESE. Reporte Técnico OC-80-02, 63 pp.

Hunter, J. R., 1980. User's manual for two-dimensional numerical hydro-dynamical model. Unit for the Coastal and Estuarine Studies. Marine Science Laboratories, Menai Bridge, Anglesey. Report U80-5, 23 pp.

Ocampo Torres, F. J., 1983. Circulación en Bahía de Todos Santos. Universidad Autónoma de Baja California. Reporte de Datos 83-01, 44 pp.

Phillips, O. M., 1977. The Dynamics of the Upper Ocean. Cambridge at the University press, 261 pp.

Reid, J. L., R. I. Roden and J. G. Wyllie, 1958. Studies of the California Current System. Prog. Rep. California Cooperative Oceanic Fisheries Investigation. 1 July 1956 - 1 January 1958, 27-56.

Reyes, S., G. Vogel, E. Pavia y A. Pares, 1983. Synoptic effects on the local winds in Todos Santos Bay: A case study. *Mon. Wea. Rev.*, **111**, 1494-1500.

Sañudo Wilhelmy, y J. A. Vargas Flores, 1984. Contaminación Fecal en la Bahía de Ensenada, B. C., México. *Ciencias Marinas*, **10**(1), 7-12.

Weyl, P. K., 1976. Pollution Suceptibility: An environmental parameter for coastal zone management. *Journal of Coastal Zone Management*, **2**, 327-343.